Neutrinoless double-electron capture

J. Kotila,[1,2,*] J. Barea,[3,†] and F. Iachello[1,‡]

[1]*Center for Theoretical Physics, Sloane Physics Laboratory, Yale University, New Haven, Connecticut 06520-8120, USA*
[2]*Department of Physics, University of Jyväskylä, B.O. Box 35, FIN-40014, Jyväskylä, Finland*
[3]*Departamento de Física, Universidad de Concepción, Casilla 160-C, Concepción 4070386, Chile*

Direct determination of the neutrino mass is at the present time one of the most important aims of experimental and theoretical research in nuclear and particle physics. A possible way of detection is through neutrinoless double-electron capture, 0νECEC. This process can only occur when the energy of the initial state matches precisely that of the final state. We present here a calculation of prefactors (PFs) and nuclear matrix elements (NMEs) within the framework of the microscopic interacting boson model (IBM-2) for ^{124}Xe, ^{152}Gd, ^{156}Dy, ^{164}Er, and ^{180}W. From the PF and NME we calculate the expected half-lives and obtain results that are of the same order as those of $0\nu\beta^+\beta^+$ decay, but considerably longer than those of $0\nu\beta^-\beta^-$ decay.

I. INTRODUCTION

The question of whether or not the neutrino is a Majorana particle and, if so, what is its average mass remains one of the most fundamental problems in physics today. In a previous series of papers we calculated the phase-space factors (PSFs) and nuclear matrix elements (NMEs) for $0\nu\beta^-\beta^-$, $2\nu\beta^-\beta^-$ processes [1–9], and for $0\nu\beta^+\beta^+$, 0νECβ^+, and $2\nu\beta^+\beta^+$, 2νECβ^+, and 2νECEC processes [10,11]. The PSFs and NMEs for the neutrinoless double-electron capture (0νECEC) process were not calculated because, in general, one cannot conserve energy and momentum in the process

$$(A,Z) + 2e^- \rightarrow (A,Z-2). \tag{1}$$

However, conservation of energy and momentum can occur in the special case in which the energy of the initial state matches precisely the energy of the final state. This situation was first discussed by Winter [12] and subsequently elaborated by Bernabeu *et al.* [13], who provided estimates of the inverse lifetimes with simple NMEs and prefactors (PFs). The work in [13] stimulated many experimental searches and additional theoretical papers [14–37]. The process was also termed resonant neutrinoless double-electron capture, R0νECEC. The matching condition can occur either for g.s. to g.s. transitions or for transitions between the g.s. and an excited state in the final nucleus. The precise matching condition is an exceptional circumstance which may or may not occur in practice. A slightly less stringent condition is that the decay occurs through the tail of the width of the atomic initial state as shown schematically in Fig. 1. For this process, depicted in Fig. 2, the inverse half-life can be to a good approximation factorized as [13]

$$\left[\tau_{1/2}^{\text{ECEC}}(0^+)\right]^{-1} = g_A^4 G_{0\nu}^{\text{ECEC}} \left|M_{\text{ECEC}}^{0\nu}\right|^2 |f(m_i,U_{ei})|^2 \frac{(m_e c^2)\Gamma}{\Delta^2 + \Gamma^2/4}, \tag{2}$$

where $G_{0\nu}^{\text{ECEC}}$ is a prefactor depending on the probability that a bound electron is found at the nucleus (see Sec. II), $M_{\text{ECEC}}^{0\nu}$ is the nuclear matrix element, and $f(m_i,U_{ei})$ contains physics beyond the standard model through the masses m_i and mixing matrix elements U_{ei} of neutrino species. For light-neutrino exchange,

$$f(m_i,U_{ei}) = \frac{\langle m_\nu \rangle}{m_e}, \quad \langle m_\nu \rangle = \sum_{k=\text{light}} (U_{ek})^2 m_k, \tag{3}$$

while for heavy-neutrino exchange,

$$f(m_i,U_{ei}) = m_p \langle m_{\nu_h}^{-1} \rangle, \quad \langle m_{\nu_h}^{-1} \rangle = \sum_{k=\text{heavy}} \left(U_{ek_h}\right)^2 \frac{1}{m_{k_h}}. \tag{4}$$

The last factor, often written as

$$\frac{(m_e c^2)\Gamma}{\Delta^2 + \Gamma^2/4} = (m_e c^2)F, \tag{5}$$

is the figure of merit for this process. Here $\Delta = |Q - B_{2h} - E|$ is called the degeneracy parameter, where $\Gamma = \Gamma_{e_1} + \Gamma_{e_2}$ is
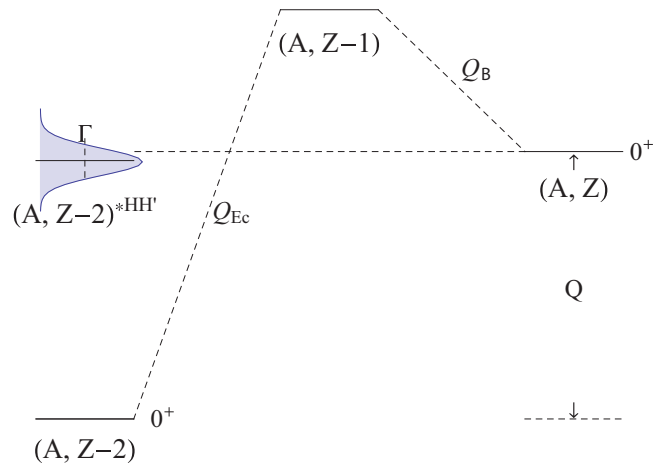

FIG. 1. (Color online) Schematic representation of neutrinoless double-electron capture.

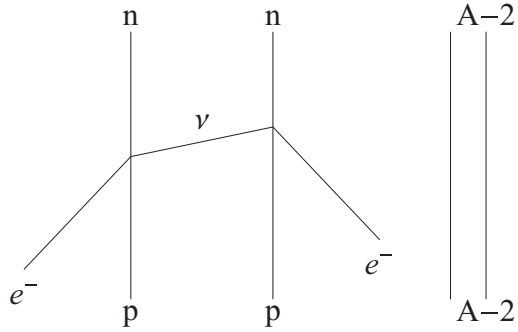*jenni.kotila@yale.edu
†jbarea@udec.cl
‡francesco.iachello@yale.edu

FIG. 2. Neutrinoless double-electron capture where $\nu = \bar{\nu}$ can be either a light or heavy neutrino.

FIG. 3. Energetics of ^{152}Gd $\rightarrow$ ^{152}Sm double-electron capture.

the two-hole width and B_{2h} is the energy of the double-electron hole in the atomic shell of the daughter nuclide including binding energies and Coulomb interaction energy. The importance of the Coulomb interaction energy of the two holes was investigated in Ref. [21]. Obviously the maximum value of F is $F^{\max} = 4/\Gamma$.

Since Γ is of the order of eV one needs to find nuclei or nuclear states such that Δ has the smallest possible value. This requires an accurate measurement of the Q value. Recent improvements in measurements of mass differences [18,19,22–24,33,34] have ruled out many of the initial candidates. In this paper, we report calculations of the PFs and NMEs of the five remaining candidates, ^{124}Xe $\rightarrow$ ^{124}Te*, ^{152}Gd $\rightarrow$ ^{152}Sm, ^{156}Dy $\rightarrow$ ^{156}Gd*, ^{164}Er $\rightarrow$ ^{164}Dy, and ^{180}W $\rightarrow$ ^{180}Hf, where the star denotes the excited state. (In addition to these, other candidates remain but with spin and parity of the final excited state unknown. These cases are not discussed here.) The energetics for the five cases of interest are shown in Table I. The case ^{152}Gd $\rightarrow$ ^{152}Sm decay is also illustrated in Fig. 3.

II. PREFACTORS

In the calculation of the prefactor, PF$\equiv G_{0\nu}^{\mathrm{ECEC}}$, we follow the theory described in our previous papers [2,10], in particular

that of [10] for electron capture (EC). The captured electrons are described by positive-energy Dirac central field bound-state wave functions,

$$\psi_{n'\kappa\mu}(\mathbf{r}) = \begin{pmatrix} g_{n',\kappa}^b(r)\chi_\kappa^\mu \\ if_{n',\kappa}^b(r)\chi_{-\kappa}^\mu, \end{pmatrix}, \qquad (6)$$

where n' denotes the radial quantum number and the quantum number κ is related to the total angular momentum, $j_\kappa = |\kappa| - 1/2$. The bound-state wave functions are normalized in the usual way:

$$\int \psi_{n'\kappa\mu}(\mathbf{r})^\dagger \psi_{n'\kappa\mu}(\mathbf{r})d\mathbf{r}$$

$$= \int_0^\infty \left[\left(g_{n',\kappa}^b(r) \right)^2 + \left(f_{n',\kappa}^b(r) \right)^2 \right] dr = 1. \qquad (7)$$

They are calculated numerically by solving the Dirac equation with finite nucleon size and electron screening in the Thomas-Fermi approximation [2,10].

For the calculation of electron capture processes the crucial quantity is the probability that an electron is found at the

TABLE I. Double-electron captures considered, Q value of the decay, energy of the resonant state in the daughter nucleus, capture shells, energy of the double-electron hole, two-hole width, and resonance enhancement factor.

Decay	Q value (keV)	E(keV)	$Q - E$(keV)	Shells	B_{2h}(keV)	Δ(keV)	Γ(keV)[a]	$(m_e c^2)F$
$^{124}_{54}$Xe$_{70} \rightarrow {}^{124}_{52}Te^*_{72}$	2856.73 ± 0.12[b]	2790.41 ± 0.09	66.32	$K - K$	64.457[b]	1.86	0.0198	2.92
$^{152}_{64}$Gd$_{88} \rightarrow {}^{152}_{62}Sm_{90}$	55.70 ± 0.18[c]	0.0	55.70	$K - L_1$	54.795[c]	0.91	0.023	14.38
$^{156}_{66}$Dy$_{90} \rightarrow {}^{156}_{64}Gd^*_{92}$	2005.95 ± 0.10[d]	1988.5 ± 0.2	17.45	$L_1 - L_1$	16.914[d]	0.54	0.0076	13.52
$^{164}_{68}$Er$_{96} \rightarrow {}^{164}_{66}Dy_{98}$	25.07 ± 0.12[e]	0.0	25.07	$L_1 - L_1$	18.259[e]	6.81	0.0086	0.095
$^{180}_{74}$W$_{106} \rightarrow {}^{180}_{72}Hf_{108}$	143.20 ± 0.27[f]	0.0	143.20	$K - K$	131.96[gh]	11.24	0.072	0.29

[a]Ref. [38].
[b]Ref. [33].
[c]Ref. [25].
[d]Ref. [26].
[e]Ref. [27].
[f]Ref. [35].
[g]Ref. [39].
[h]Ref. [21].

TABLE II. Prefactors for neutrinoless double-electron capture.

Decay	$G_{0\nu}^{\mathrm{ECEC}}(10^{-19}\mathrm{yr}^{-1})$	
	This work	Ref. [21]
$^{124}_{54}\mathrm{Xe}_{70} \rightarrow {}^{124}_{52}\mathrm{Te}^*_{72}$	2.57	
$^{152}_{64}\mathrm{Gd}_{88} \rightarrow {}^{152}_{62}\mathrm{Sm}_{90}$	1.46	1.67
$^{156}_{66}\mathrm{Dy}_{90} \rightarrow {}^{156}_{64}\mathrm{Gd}^*_{92}$	0.266	0.22
$^{164}_{68}\mathrm{Er}_{96} \rightarrow {}^{164}_{66}\mathrm{Dy}_{98}$	0.362	0.31
$^{180}_{74}\mathrm{W}_{106} \rightarrow {}^{180}_{72}\mathrm{Hf}_{108}$	46.2	34.9

nucleus. This can be expressed in terms of the dimensionless quantity

$$\mathcal{B}^2_{n',\kappa} = \frac{1}{4\pi(m_ec^2)^3}\left(\frac{\hbar c}{a_0}\right)^3\left(\frac{a_0}{R}\right)^2\left[(g^b_{n',\kappa}(R))^2 + (f^b_{n',\kappa}(R))^2\right],$$
(8)

where a_0 is the Bohr radius $a_0 = 0.529 \times 10^{-8}$cm, and we use for the nuclear radius $R = 1.2A^{1/3}$fm. For capture from the K shell $n' = 0$, $\kappa = -1$, $1S_{1/2}$; while for capture from the L_I shell $n' = 1$, $\kappa = -1$, $2S_{1/2}$. The PF is given by

$$G_{0\nu}^{\mathrm{ECEC}} = \frac{1}{4R^2\ln 2}\frac{(G\cos\theta)^4}{2\pi^2}(\hbar c^2)(m_ec^2)^7\mathcal{B}^2_{n'_{e_1},-1}\mathcal{B}^2_{n'_{e_2},-1}.$$
(9)

The obtained prefactors are listed in Table II.

Recently Krivoruchenko *et al.* [21] have presented a theory of PF slightly different from ours. The PF extracted from their paper is given in the last column of Table II for comparison. Note the large value of $G_{0\nu}^{\mathrm{ECEC}}$ in both calculations for ^{180}W decay, due to the large value of $Z\alpha = 74/137 \sim 0.5$. For these heavy nuclei the PF is very sensitive to the treatment of

the electron wave function near the origin $r = 0$. Differences between the two PF calculations may in part arise from the way in which the nuclear size and electron screening correction are taken into account.

III. NUCLEAR MATRIX ELEMENTS

The calculation of NMEs for the 0νECEC is more difficult than for $0\nu\beta^-\beta^-$ because of two reasons: (i) In the two cases ^{124}Xe and ^{156}Dy the resonant state is an excited state. (ii) In the other cases, the decay ^{152}Gd is to a transitional nucleus, and the decays ^{164}Er and ^{180}W are to strongly deformed nuclei. For these reasons, one needs a model that can calculate reliably energies and wave functions of ground and excited states in spherical, transitional, and deformed nuclei. To this end we make use of the microscopic interacting boson model (IBM-2) [40]. The method is described in Refs. [1,4]. We write

$$M_{0\nu} = g_A^2 M^{(0\nu)}, \quad M^{(0\nu)} = M_{\mathrm{GT}}^{(0\nu)} - \left(\frac{g_V}{g_A}\right)^2 M_F^{(0\nu)} + M_T^{(0\nu)},$$
(10)

with $M_{\mathrm{GT}}^{(0\nu)}$, $M_F^{(0\nu)}$, and $M_T^{(0\nu)}$ defined as in Eq. (20) of Ref. [4]

$$M_{\mathrm{GT}}^{(0\nu)} \equiv \langle {}^AX;0^+_1|h^{\mathrm{GT}}(p)/g_A^2|{}^AY;J_F\rangle,$$
$$M_F^{(0\nu)} \equiv \langle {}^AX;0^+_1|h^F(p)/g_V^2|{}^AY;J_F\rangle,$$
(11)
$$M_T^{(0\nu)} \equiv \langle {}^AX;0^+_1|h^T(p)/g_A^2|{}^AY;J_F\rangle,$$

where $h(p)$ are the form factors tabulated in Table II of [4]. The wave functions of the initial and final states are taken either from the literature or from a fit to the observed energies and other properties [$B(E2)$ values, quadrupole moments, $B(M1)$ values, magnetic moments, etc.]. The values of the parameters used in the calculation are given in the Appendix. The quality of the wave functions as well as the quality of the description
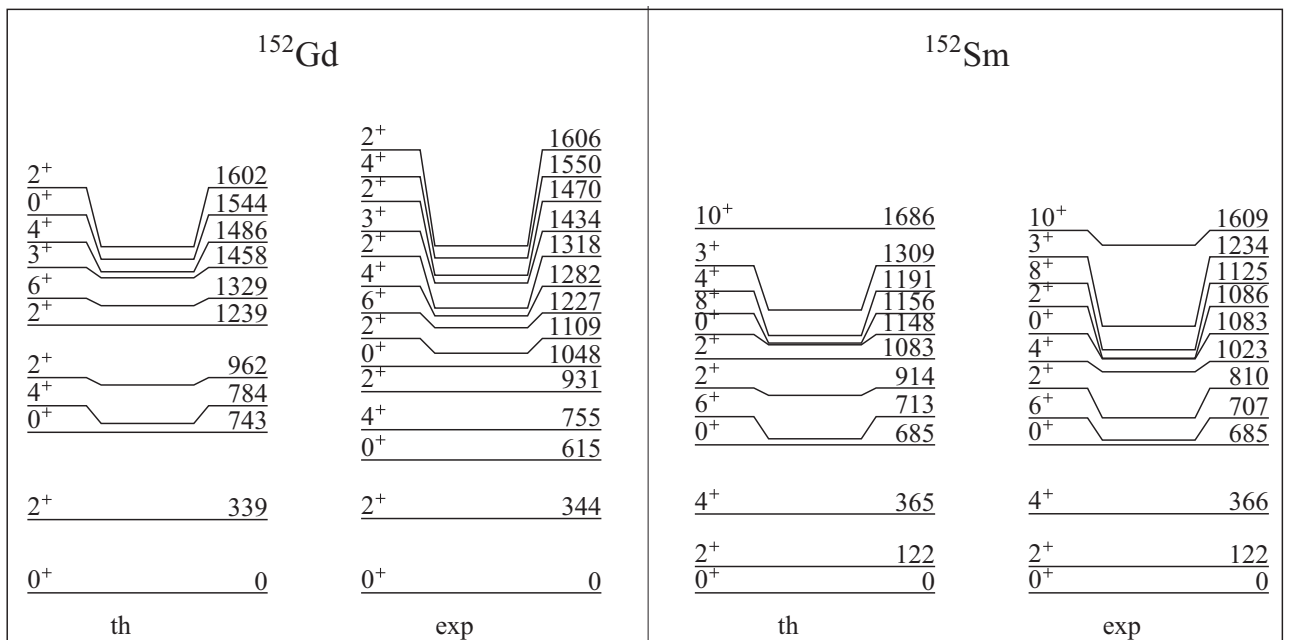

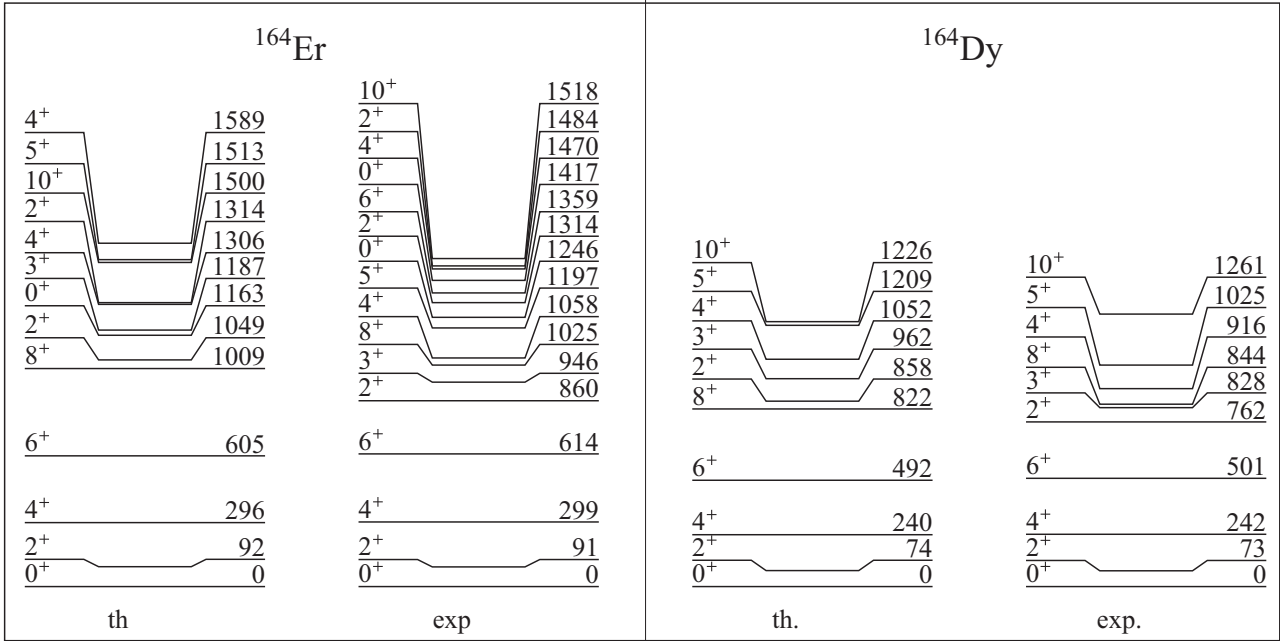FIG. 4. Comparison between calculated and experimental low-lying spectra for ^{152}Gd $\rightarrow$ ^{152}Sm.

FIG. 5. Comparison between calculated and experimental low-lying spectra for ^{164}Er $\rightarrow$ ^{164}Dy.

of energies and electromagnetic transition rates is excellent both in transitional $A = 152$, Fig. 4, and strongly deformed $A = 164$, Fig. 5, and $A = 180$, Fig. 6, nuclei.

For decays to excited states, particular care must be taken in identifying the state in the calculated spectrum. For decay to ^{156}Gd this state is the 0_4^+ state calculated at 1988 keV, while for decay to ^{124}Te this state is also the 0_4^+ state calculated at 2790 keV. The quality of the excited spectrum of states in ^{124}Te, Fig. 7, and ^{156}Gd, Fig. 8, is also excellent.

Using IBM-2 wave functions and the theory previously described [1,4] we can calculate the NMEs for neutrinoless ECEC decay shown in Table III. The values of the nuclear matrix elements to the excited states are considerably smaller than those to the ground state, due to the very different nature of these states. To illustrate this point we show in Table IV the results of the calculation for $A = 156$ leading to the first five 0^+ states in ^{156}Gd. We see that the matrix elements of 0_3^+, 0_4^+, and 0_5^+ are one order of magnitude smaller than 0_1^+

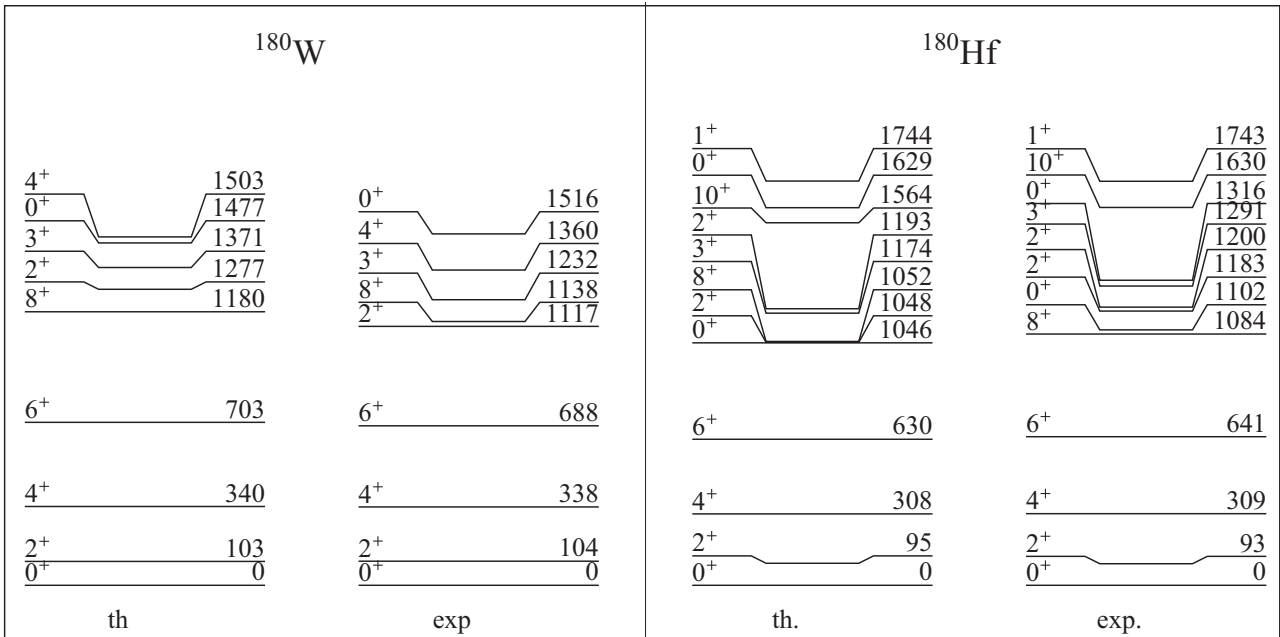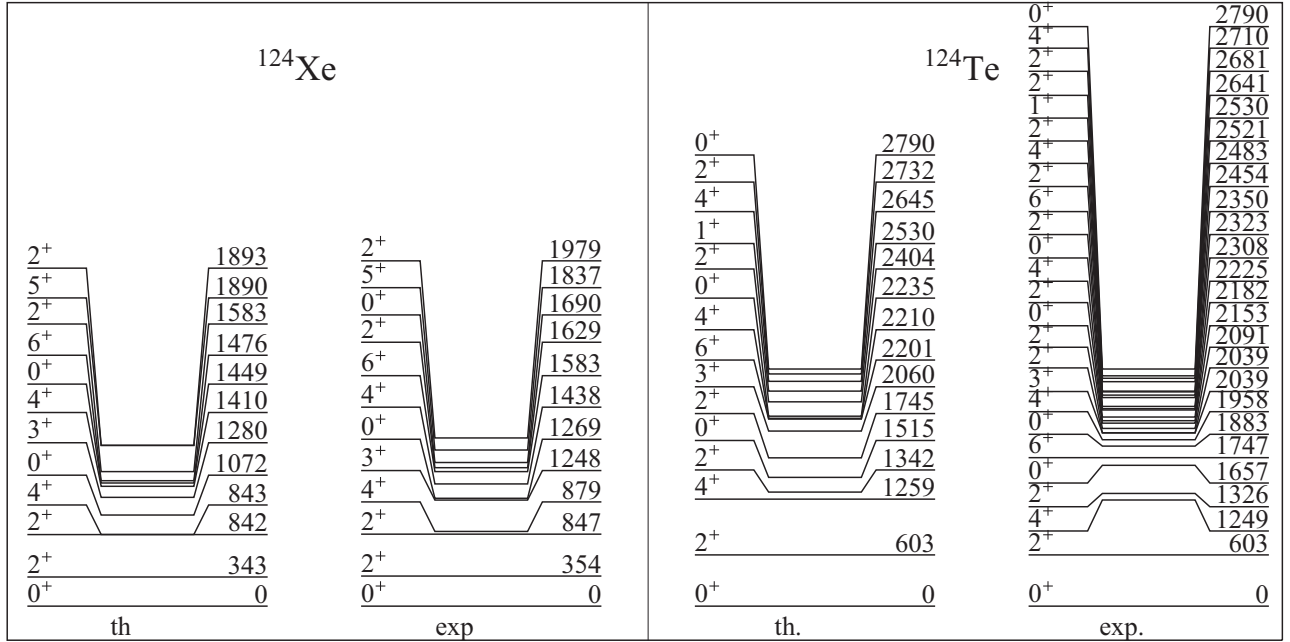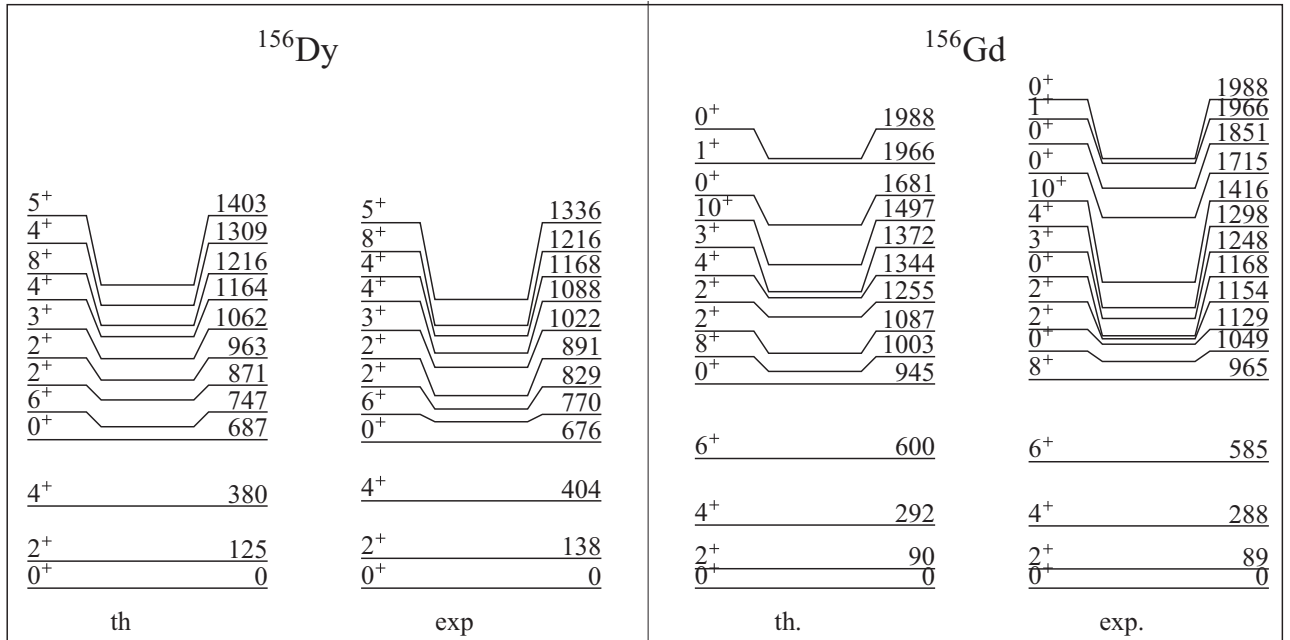FIG. 6. Comparison between calculated and experimental low-lying spectra for ^{180}W $\rightarrow$ ^{180}Hf.

FIG. 7. Comparison between calculated and experimental low-lying spectra for ^{124}Xe $\rightarrow$ ^{124}Te.

FIG. 8. Comparison between calculated and experimental low-lying spectra for ^{156}Dy $\rightarrow$ ^{156}Gd.

TABLE III. IBM-2 nuclear matrix elements $M^{(0\nu)}$ (dimensionless) for neutrinoless ECEC decay with the Argonne short-range correlation (SRC) and $g_V/g_A = 1/1.269$.

	$M^{(0\nu)}$ light				$M_h^{(0\nu)}$ heavy			
	$M_{GT}^{(0\nu)}$	$M_F^{(0\nu)}$	$M_T^{(0\nu)}$	$M^{(0\nu)}$	$M_{GT}^{(0\nu)}$	$M_F^{(0\nu)}$	$M_T^{(0\nu)}$	$M_h^{(0\nu)}$
^{124}Xe $\rightarrow$ ^{124}Te*[0_4^+]	0.277	-0.051	-0.012	0.297	6.447	-2.921	-1.521	6.740
^{152}Gd $\rightarrow$ ^{152}Sm[0_1^+]	2.132	-0.352	0.095	2.445	68.910	-31.400	12.810	101.200
^{156}Dy $\rightarrow$ ^{156}Gd*[0_4^+]	0.265	-0.048	0.017	0.311	10.530	-4.739	2.616	16.090
^{164}Er $\rightarrow$ ^{164}Dy[0_1^+]	3.456	-0.444	0.221	3.952	107.900	-46.820	32.870	169.800
^{180}W $\rightarrow$ ^{180}Hf[0_1^+]	4.117	-0.566	0.204	4.672	118.700	-53.320	28.200	170.900

TABLE IV. IBM-2 nuclear matrix elements $M^{(0\nu)}$ (dimensionless) for $A = 156$ neutrinoless ECEC decay to the first five 0^+ states with the Argonne SRC and $g_V/g_A = 1/1.269$.

	$M^{(0\nu)}$ light				$M_h^{(0\nu)}$ heavy			
	$M_{GT}^{(0\nu)}$	$M_F^{(0\nu)}$	$M_T^{(0\nu)}$	$M^{(0\nu)}$	$M_{GT}^{(0\nu)}$	$M_F^{(0\nu)}$	$M_T^{(0\nu)}$	$M_h^{(0\nu)}$
0_1^+	2.796	−0.398	0.132	3.175	82.560	−36.990	17.480	123.000
0_2^+	1.532	−0.227	0.076	1.749	47.630	−21.360	10.430	71.320
0_3^+	0.403	−0.065	0.022	0.466	13.900	−6.242	3.225	21.000
0_4^+	0.265	−0.048	0.017	0.311	10.530	−4.739	2.616	16.090
0_5^+	0.302	−0.046	0.016	0.346	9.809	−4.402	2.204	14.750

and 0_2^+. This has a major consequence on 0νECEC essentially excluding as possible candidates all decays to excited states. A similar conclusion was drawn in Ref. [30] for the decay ^{96}Ru → ^{96}Mo*.

NMEs to the g.s of ^{152}Sm, ^{164}Dy, and ^{180}Hf for light-neutrino exchange have also been calculated in a variety of methods. In Table V we compare our results to these other calculations. While the quasiparticle random-phase approximation (QRPA) matrix elements are of the same order of magnitude as IBM-2, the energy density functional (EDF) results are much smaller, in particular they show a large reduction for the deformed nuclei ^{164}Dy, and ^{180}Hf. The origin of this discrepancy between IBM-2/QRPA and EDF is not clear. As shown in Fig. 6 the quality of the spectrum (and the electromagnetic transitions not shown) in IBM-2 is excellent including the location of the β and γ bands, which is crucial for providing good wave functions of collective states. Also the collective structure of the parent nucleus ^{180}W and daughter nucleus ^{180}Hf is practically identical, with a large overlap, and both nuclei have many collective pairs, $N_\pi = 4$ or 5 and $N_\nu = 10$ or 9, respectively, that contribute to the decay. Although there is a reduction in the NME due to the deformation, we still would expect the matrix elements to be comparable to those in spherical nuclei.

IV. HALF-LIVES

The results for PF and NME of the previous sections can be combined to give the half-lives in Table VI and Figs. 9 and 10. The best case scenarios appear to be ^{152}Gd → ^{152}Sm[0_1^+] and

TABLE V. Comparison between IBM-2 matrix elements with the Argonne SRC for 0νECEC decay and QRPA and EDF.

Decay	$M^{(0\nu)}$ (light)			
	IBM-2	Spherical QRPA[a]	Deformed QRPA[a]	EDF[b]
$^{152}_{64}$Gd$_{88}$ → $^{152}_{62}$Sm$_{90}$	2.44	7.59	3.23-2.67	1.07-0.89
$^{164}_{68}$Er$_{96}$ → $^{164}_{66}$Dy$_{98}$	3.95	6.12	2.64-2.27	0.64-0.50
$^{180}_{74}$W$_{106}$ → $^{180}_{72}$Hf$_{108}$	4.67	5.79	2.05-1.79	0.58-0.38

[a]Ref. [32].
[b]Ref. [31].

^{180}W → ^{180}Hf[0_1^+], for which, however, the predicted half-life even with unquenched value of $g_A = 1.269$ is of the order of 10^{27} yr.

As in the previous papers, an important question is the quenching of the g_A which occurs to the fourth power in Eq. (2). To estimate this effect we use the parametrization of Eq. (40) of Ref. [4] (maximal quenching)

$$g_{A,\mathrm{eff}}^{\mathrm{IBM}-2} = 1.269 A^{-0.18}. \tag{12}$$

With this parametrization we obtain the values of Table VI (right).

V. CONCLUSIONS

In this paper, we have presented both PFs and NMEs for neutrinoless double-electron capture and from these calculated the expected half-lives for both light- and heavy-neutrino exchange. The values obtained are longer than those for $0\nu\beta^-\beta^-$ decay. The best cases are those of ^{180}W → ^{180}Hf[0_1^+] and ^{152}Gd → ^{152}Sm[0_1^+], where for light-neutrino exchange $\tau_{1/2} = 3.44 \times 10^{27}$ yr and 8.03×10^{27} yr, respectively, for $\langle m_\nu \rangle = 1$ eV and $g_A = 1.269$. For comparison $0\nu\beta^-\beta^-$ decays have $\tau_{1/2}$ of the order of 10^{24} yr. The half-lives for 0νECEC are, however, of the same order of magnitude of $0\nu\beta^+\beta^+$, the best case for this decay being that of ^{124}Xe → ^{124}Te which has $\tau_{1/2} = 3.32 \times 10^{27}$ yr. Our conclusion is that even in the

TABLE VI. Left: Calculated half-lives in IBM-2 for neutrinoless double-electron capture with light-neutrino exchange for $\langle m_\nu \rangle = 1$ eV and heavy neutrino exchange with $m_p \langle m_{\nu_h}^{-1} \rangle = 2.75 \times 10^{-7}$, and using unquenched value $g_A = 1.269$. Right: Same as right but using maximally quenched value $g_{A,\mathrm{eff}}^{\mathrm{IBM}-2} = 1.269 A^{-0.18}$.

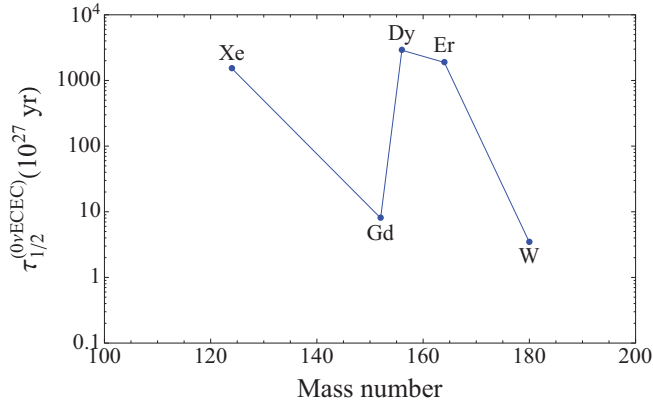| Nucleus	$\tau_{1/2}(10^{27})$yr			
	Unquenched		Maximally quenched	
	Light	Heavy	Light	Heavy
^{124}Xe → ^{124}Te*[0_4^+]	1520	150	49000	4820
^{152}Gd → ^{152}Sm[0_1^+]	8.03	0.237	298	8.83
^{156}Dy → ^{156}Gd*[0_4^+]	2890	54.7	110000	2080
^{164}Er → ^{164}Dy[0_1^+]	1880	51.6	74000	2030
^{180}W → ^{180}Hf[0_1^+]	3.44	0.131	144	5.47

FIG. 9. (Color online) Expected half-lives for light-neutrino exchange with $\langle m_\nu \rangle = 1$eV, $g_A = 1.269$. The figure is in semilogarithmic scale.
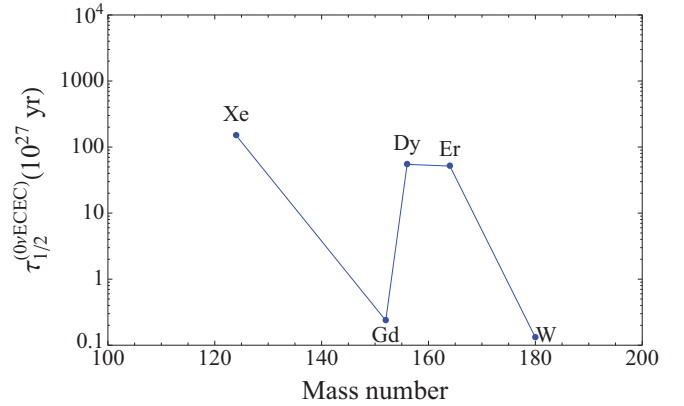

FIG. 10. (Color online) Expected half-lives for heavy-neutrino exchange with $m_p \langle m_{\nu_h}^{-1} \rangle = 2.75 \times 10^{-7}$, $g_A = 1.269$. The figure is in semilogarithmic scale.

optimistic scenario of $g_A = 1.269$, 0νECEC is unreachable in the present generation of experiments.

APPENDIX: PARAMETERS OF THE IBM-2 HAMILTONIAN

A detailed description of the IBM-2 Hamiltonian is given in Refs. [41,42]. For ^{124}Xe, ^{152}Gd, ^{156}Dy, ^{156}Gd, and ^{164}Gd the Hamiltonian parameters are taken from the literature. The new calculations are done using the program NPBOS [42] adapted by Kotila. The values of the Hamiltonian parameters, as well as the references from which they are taken, are given in Table VII.

TABLE VII. Hamiltonian parameters employed in the IBM-2 calculation along with their references.

Nucleus	$\epsilon_{d_\nu} = \epsilon_{d_\pi}$	κ	χ_ν	χ_π	ξ_1	ξ_2	ξ_3	$c_\nu^{(0)}$	$c_\nu^{(2)}$	$c_\nu^{(4)}$	$c_\pi^{(0)}$	$c_\pi^{(2)}$	$c_\pi^{(4)}$	$\omega_{\nu\nu}$	$\omega_{\pi\pi}$	$\omega_{\nu\pi}$
^{124}Xe [43]	0.70	-0.14	0.00	-0.80	-0.18	0.24	-0.18	0.05	-0.16							
^{124}Te[a]	0.83	-0.15	0.00	-1.20	-0.34	0.15	-0.34	0.10								
^{152}Gd [44]	0.74	-0.076	-0.80	-1.00	0.08	0.08	0.08				-0.20	0.10				
^{152}Sm[a]	0.52	-0.075	-1.00	-1.30	0.3	-0.01	0.03					0.05				
^{156}Dy [44]	0.62	-0.078	-1.00	-0.80	0.08	0.08	0.08				-0.05	-0.15				
^{156}Gd [44]	0.59	-0.08	-1.10	-1.00	0.11	0.09	0.11				-0.20	-0.10		-0.0025	-0.0025	-0.0025
^{164}Er[a]	0.47	-0.08	-0.50	0.70	0.24	0.24	0.24	-0.28								
^{164}Dy [44]	0.54	-0.05	-0.70	-0.80	0.17	0.17	0.17					-0.15				
^{180}W[a]	0.53	-0.11	-0.10	-1.60	-0.02	0.04	-0.02	-0.11								
^{180}Hf[a]	0.53	-0.08	-0.3	-1.20	0.05	0.05	0.05	-0.14								

[a]Parameters fitted to reproduce the spectroscopic data.

[1] J. Barea and F. Iachello, Phys. Rev. C **79**, 044301 (2009).

[2] J. Kotila and F. Iachello, Phys. Rev. C **85**, 034316 (2012).

[3] J. Barea, J. Kotila, and F. Iachello, Phys. Rev. Lett. **109**, 042501 (2012).

[4] J. Barea, J. Kotila, and F. Iachello, Phys. Rev. C **87**, 014315 (2013).

[5] J. Barea and J. Kotila, AIP Conf. Proc. **1488**, 334 (2012).

[6] J. Kotila and J. Barea, AIP Conf. Proc. **1488**, 342 (2012).

[7] D. Fink *et al.*, Phys. Rev. Lett. **108**, 062502 (2012).

[8] J. Beller *et al.*, Phys. Rev. Lett. **111**, 172501 (2013).

[9] F. Iachello, J. Barea, and J. Kotila, Nucl. Phys. B **237-238**, 21 (2013).

[10] J. Kotila and F. Iachello, Phys. Rev. C **87**, 024313 (2013).

[11] J. Barea, J. Kotila, and F. Iachello, Phys. Rev. C **87**, 057301 (2013).

[12] R. G. Winter, Phys. Rev. **100**, 142 (1955).

[13] J. Bernabeu, A. de Rujula, and C. Jarlskog, Nucl. Phys. B **223**, 15 (1983).

[14] Z. Sujkowski and S. Wycech, Phys. Rev. C **70**, 052501(R) (2004).

[15] L. Lukaszuk, Z. Sujkowski, and S. Wycech, Eur. Phys. J. A **27**, 63 (2006).

[16] P. Belli *et al.*, Nucl. Phys. A **824**, 101 (2009).

[17] F. Šimkovic and M. I. Krivoruchenko, Phys. Part. Nucl. Lett. **6**, 298 (2009).

[18] S. Rahaman *et al.*, Phys. Rev. Lett. **103**, 042501 (2009).

[19] V. S. Kolhinen *et al.*, Phys. Lett. B **684**, 17 (2010).

[20] P. Belli *et al.*, Eur. Phys. J. A **47**, 91 (2011).

[21] M. I. Krivoruchenko, F. Šimkovic, D. Frekers, and A. Faessler, Nucl. Phys. A **859**, 140 (2011).

[22] S. Eliseev *et al.*, Phys. Rev. C **83**, 038501 (2011).

[23] V. S. Kolhinen *et al.*, Phys. Lett. B **697**, 116 (2011).

[24] M. Goncharov *et al.*, Phys. Rev. C **84**, 028501 (2011).

[25] S. Eliseev *et al.*, Phys. Rev. Lett. **106**, 052504 (2011).

[26] S. Eliseev *et al.*, Phys. Rev. C **84**, 012501(R) (2011).

[27] S. Eliseev *et al.*, Phys. Rev. Lett. **107**, 152501 (2011).

[28] J. D. Vergados, Phys. Rev. C **84**, 044328 (2011).

[29] J. Suhonen, Eur. Phys. J. A **48**, 51 (2012).

[30] J. Suhonen, Phys. Rev. C **86**, 024301 (2012).

[31] T. R. Rodríguez and G. Martínez-Pinedo, Phys. Rev. C **85**, 044310 (2012).

[32] D.-L. Fang, K. Blaum, S. Eliseev, A. Faessler, M. I. Krivoruchenko, V. Rodin, and F. Šimkovic, Phys. Rev. C **85**, 035503 (2012).

[33] D. A. Nesterenko *et al.*, Phys. Rev. C **86**, 044313 (2012).

[34] C. Smorra *et al.*, Phys. Rev. C **86**, 044604 (2012).

[35] C. Droese *et al.*, Nucl. Phys. A **875**, 1 (2012).

[36] P. Belli *et al.*, Eur. Phys. J. A **49**, 24 (2013).

[37] J. Suhonen, J. Phys. G **40**, 075102 (2013).

[38] J. L. Campbell and T. Papp, At. Data Nucl. Data Tables **77**, 1 (2001).

[39] F. B. Larkins, At. Data Nucl. Data Tables **20**, 311 (1977).

[40] F. Iachello and A. Arima, *The Interacting Boson Model* (Cambridge University, Cambridge, England, 1987).

[41] A. Arima, T. Otsuka, F. Iachello, and I. Talmi, Phys. Lett. B **66**, 205 (1977).

[42] T. Otsuka and N. Yoshida, User's Manual of the Program NPBOS, Report No. JAERI-M 85-094, 1985.

[43] G. Puddu, O. Scholten, and T. Otsuka, Nucl. Phys. A **348**, 109 (1980).

[44] J. Kotila, K. Nomura, L. Guo, N. Shimizu, and T. Otsuka, Phys. Rev. C **85**, 054309 (2012), and private communication.